

Modulated point-vortex pairs on a rotating sphere: Dynamics and chaotic advectionGábor Drótos,¹ Tamás Tél,^{1,2} and Gergely Kovács¹¹*Institute of Theoretical Physics, Eötvös University, Pázmány Péter sétány 1/A, H-1117 Budapest, Hungary*²*Research Group in Theoretical Physics of the Hungarian Academy of Sciences at Eötvös University, Pázmány Péter sétány 1/A, H-1117 Budapest, Hungary*

(Received 14 December 2012; revised manuscript received 2 May 2013; published 27 June 2013)

The dynamics of modulated point-vortex pairs is investigated on a rotating sphere, where modulation is chosen to reflect the conservation of angular momentum (potential vorticity). For sufficiently close vortices (dipoles) the trajectories of their center-of-mass are shown to correspond to those of a point particle moving freely on a rotating sphere. For finite size vortex pairs, a qualitative similarity to the geodesic dynamics is found. The advection dynamics generated by vortex pairs on a rotating sphere is found to be chaotic. In the short time dynamics we point out a transition from closed to open chaotic advection, which implies that the transport properties of the flow might drastically be altered by changing the initial conditions of the pair on the sphere. Due to spherical topology, for long times, even the open advection patterns are found to gradually cross over to that corresponding to a homogeneous closed mixing. This pattern extends along a zonal band, whereas short term closed mixing remains always bounded to the moving pair.

DOI: [10.1103/PhysRevE.87.063017](https://doi.org/10.1103/PhysRevE.87.063017)

PACS number(s): 47.32.-y, 05.45.-a, 47.52.+j

I. INTRODUCTION

There is a current interest in the dynamics of point vortices on a sphere. After the appearance of Newton's book [1] and more recent reviews [2], the emphasis seems to have been shifted from nonrotating to rotating spheres [3–6] due to an increasing focus on environmental and climatic aspects of hydrodynamical flows.

The precise description of the vortex dynamics on a rotating sphere requires the proper handling of the interaction between the vorticity and the background flow. This is possible only in the form of an integrodifferential or a partial differential equation (see, e.g., Ref. [7]). In order to keep the low-dimensional character of the usual point-vortex dynamics, a widely used approximation [2–5] considers a solid body rotation with the angular velocity of the sphere as the background flow and neglects the feedback of the point vortices of constant circulation on the background flow. In this setting the conservation of the fluid's angular momentum (which appears in the hydrodynamical context via the so-called potential vorticity) cannot be clearly incorporated.

Another, phenomenological approach in which this drawback can be avoided is based on a modulation of the vortex circulations. Motivated by vortices moving over sloping bottoms, there is an extended literature [8–12] on how the conservation of potential vorticity [13] can be introduced into the point-vortex picture by applying a modulation of the vortex circulation with the coordinate along the slope. The circulation Γ_j of any vortex is made linearly location dependent. This is done in the spirit of the β -plane approximation [11,13], according to which the local vertical component of the Earth's angular velocity (responsible for Coriolis deflection) can be considered to depend linearly on the latitudinal angle φ . With this approach, one neglects the vorticity production due to the transport of fluid elements outside the vortices, as discussed in Ref. [11,13]. The modulated point-vortex model is therefore valid as long as this vorticity gain is negligible. The price of this approach is the introduction of a phenomenological quantity, called the vortex radius. Although such point vortices are not

exact solutions of the hydrodynamical equations, they have been shown to be useful in understanding several features, e.g., the existence of modonlike excitations [8]. In a number of experiments, laboratory-generated vortices on a topographic β plane (sloping bottom) could be approximated quite well by the modulated point-vortex model over a considerable time span [11,14–17].

Here we generalize the principle of modulation by making the vortex circulation nonlinearly dependent on the latitudinal angle φ_j of vortex j . The idea is to take into account the conservation of total vorticity on a sphere rotating with angular velocity Ω . This is valid in a shallow layer of fixed height, and implies [13]

$$\zeta(\varphi, \lambda) + 2\Omega \sin \varphi = C \quad (1)$$

along a fluid element trajectory, where ζ denotes the vertical component of the vorticity vector expressed in geographical coordinates λ (longitude) and φ (latitude), and C is a constant. Under the assumption that a point vortex represents a small patch of vorticity, of an area $a^2\pi$, the circulation of vortex j with coordinates φ_j, λ_j is given as $\Gamma_j = a^2\pi \zeta(\varphi_j, \lambda_j)$. From Eq. (1) we then obtain

$$\Gamma_j(\varphi_j) = \Gamma_{j\tau} - 2\Omega a^2\pi (\sin \varphi_j - \sin \varphi_{j\tau}), \quad (2)$$

where

$$\Gamma_{j\tau} = a^2\pi C - 2\Omega a^2\pi \sin \varphi_{j\tau} \quad (3)$$

is the circulation at a reference latitude $\varphi_{j\tau}$. We call $\Gamma_{j\tau}$ the vortex strength (at the reference latitude), and a the vortex radius, the latter being assumed to be the same for all point vortices. Equation (2) sets the modulation of circulation on a rotating sphere.

In this paper we investigate the dynamics and advective features of special two-vortex systems, vortex pairs. We see that the possible types of the center-of-mass trajectory of a vortex pair of small distance correspond to those of a point particle moving freely on a rotating sphere as described in Refs. [18–22]. The fact that the motion of vortex pairs and

that of free particles become related on a rotating sphere can be qualitatively understood based on the observation that fluid elements move approximately as free particles in the presence of weak pressure gradients [23].

Although the vortex pair dynamics is regular (but non-trivial), the advection in its velocity field is chaotic. This is only the consequence of the rotation of the sphere (since the motion of a vortex pair on a nonrotating sphere is always uniform [1]). In the character of the advection dynamics a time scale separation can be observed. On the time scale of a single winding around the sphere there is a clear transition from closed advection (tracer patterns remain bounded to the moving pair for all times) to open advection (tracers become distributed in the wake of the pair) at a critical value of the initial latitude of the center of mass of the vortex pair. Due to spherical topology, however, the vortex pair meets its wake after one winding of the sphere. Therefore, for long time scales the advection dynamics becomes closed and the wake homogeneously mixed. This pattern extends along a zonal band, whereas short-time closed mixing remains always bounded to the moving pair. An explanation of this crossover

is given in terms of the chaotic saddle, underlying any open advection problem, as becoming space filling.

In Sec. II we write the equations for modulated point vortices on a rotating sphere. Numerical results for modulated vortex pairs are shown in Sec. III. The derivation of the dipole equations is done in Sec. IV, and we compare this dynamics with that of the free particle in Sec. V. Section VI is devoted to the advection dynamics. The chaotic sets and droplet patterns are investigated both on short and long time scales. We summarize our findings in Sec. VII. Technically more involved parts are relegated to Appendices.

II. THE MODEL

We consider point vortices whose location is specified by angles λ , φ in geographical coordinates on the surface of a sphere of radius R (λ being the longitude, φ the latitude). The equations of motion for N modulated point vortices are the same as for constant-circulation vortices (see Ref. [1]) just the circulation of vortex j is given by $\Gamma_j(\varphi_j)$ as expressed in Eq. (2). We thus have

$$\frac{d\varphi_i}{dt} = \frac{1}{4\pi R^2} \sum_{j \neq i} \frac{\Gamma_j(\varphi_j) \cos \varphi_j \sin(\lambda_i - \lambda_j)}{1 - \cos \gamma_{ij}}, \quad i, j = 1, \dots, N, \quad (4a)$$

$$\frac{d\lambda_i}{dt} = \frac{1}{\cos \varphi_i} \frac{1}{4\pi R^2} \sum_{j \neq i} \frac{\Gamma_j(\varphi_j) [\cos \varphi_i \sin \varphi_j - \sin \varphi_i \cos \varphi_j \cos(\lambda_i - \lambda_j)]}{1 - \cos \gamma_{ij}}, \quad (4b)$$

where

$$\cos \gamma_{ij} = \sin \varphi_i \sin \varphi_j + \cos \varphi_i \cos \varphi_j \cos(\lambda_i - \lambda_j), \quad (5)$$

and $2R^2(1 - \cos \gamma_{ij}) = r_{ij}^2$ is the chord distance between vortices i and j .

A natural choice of the length and time scales, L and T , is obtained if the radius is taken as the length unit and $1/\Omega$ is chosen to be proportional to the time unit, i.e., $L = R$ and $T = 1/(2\Omega)$. As a consequence, the dimensionless circulations are

$$\begin{aligned} \Gamma'_j(\varphi_j) &= \Gamma'_{jr} - a^2 \pi (\sin \varphi_j - \sin \varphi_{jr}), \\ a' &= \frac{a}{R}, \quad \Gamma'_{jr} = \frac{\Gamma_{jr}}{2\Omega R^2}. \end{aligned} \quad (6)$$

From here on, we consider two modulated vortices. Their chord distance D' is a constant of motion, as shown in Appendix A. We write the dimensionless equations for two vortices by explicitly indicating that the dimensionless distance is a constant D' :

$$\frac{d\varphi_i}{dt} = \frac{[\Gamma'_{jr} - a^2 \pi (\sin \varphi_j - \sin \varphi_{jr})] \cos \varphi_j \sin(\lambda_i - \lambda_j)}{2\pi D'^2}, \quad (7a)$$

$$\begin{aligned} \frac{d\lambda_i}{dt} &= \frac{1}{\cos \varphi_i} \frac{1}{2\pi D'^2} [\Gamma'_{jr} - a^2 \pi (\sin \varphi_j - \sin \varphi_{jr})] \\ &\times [\cos \varphi_i \sin \varphi_j - \sin \varphi_i \cos \varphi_j \cos(\lambda_i - \lambda_j)]. \end{aligned} \quad (7b)$$

Here $i, j = 1, 2$, $i \neq j$, and the initial conditions are given by the initial values λ_{i0} , φ_{i0} , $i = 1, 2$. Alternatively, we can use the initial center-of-mass coordinates λ_0 , φ_0 and the initial angle, denoted by α_0 , between the line connecting the elements of the pair and the local meridian ($\lambda = \text{const}$). The value of α_0 is chosen to be 0 when vortex 1 is closer to the North Pole than vortex 2 (while both vortices are along the same $\lambda = \text{const}$ line).

We consider a type I vortex pair to be a two-vortex system whose elements have oppositely equal vortex strengths at a *common* reference latitude:

$$\varphi_{1r} = \varphi_{2r} \equiv \varphi_r \quad (8)$$

and

$$\Gamma'_{1r} = -\Gamma'_{2r} \equiv \Gamma' > 0. \quad (9)$$

This definition gives φ_r a well-defined physical meaning, and φ_r becomes an important parameter of the vortex pair model. (We note that this definition of a vortex pair permits the elements of the pair to have the same sign of circulation at latitudes far enough from the reference latitude for certain parameter values. However, in most of the cases considered in this paper, and in particular in the dipole limit, the circulations have different signs for all times.)

A type II vortex pair is defined by the opposite equivalence of the initial circulations *wherever they start*:

$$\Gamma'_1(\varphi_{10}) = -\Gamma'_2(\varphi_{20}) > 0. \quad (10)$$

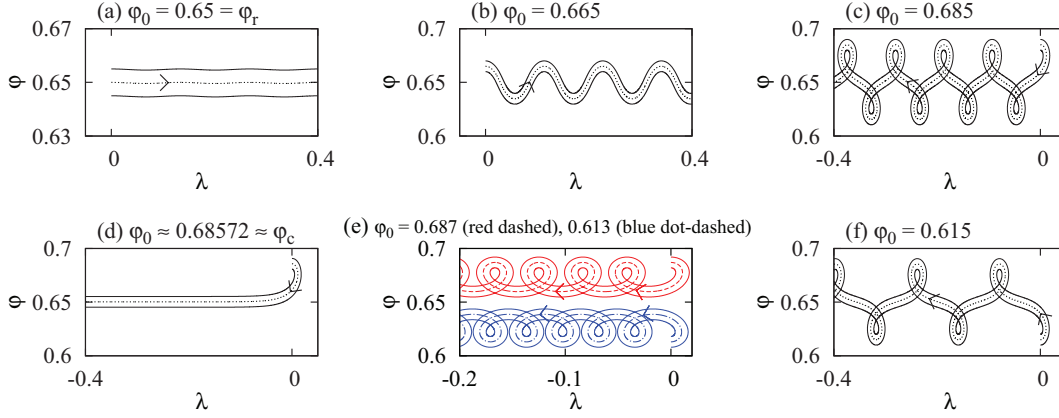


FIG. 1. (Color online) Trajectories of the vortices (solid lines) and of their centers of mass (dotted, dashed, or dot-dashed lines) on the (λ, φ) plane for type I pairs, when varying the initial latitude φ_0 . The arrows indicate the direction of propagation. Parameters: $\varphi_r = 0.65$, $D' = 0.01$, $a' = 0.01$, $\Gamma' = 5 \times 10^{-6}\pi$. Initial conditions: $\alpha_0 = 0$, $\lambda_0 = 0$, and φ_0 as indicated in the panels. The special latitude to which the trajectory of (d) converges is $\varphi_- = 0.65027$. The other special latitude (not shown) is $\varphi_+ = 0.64979$.

We identify the reference latitudes of the two vortices with their initial latitudes,

$$\varphi_{jr} = \varphi_{j0}, \quad j = 1, 2, \quad (11)$$

in order to ensure that Eq. (9) holds again. In Sec. IV we point out that both definitions lead to identical results in the dipole limit.

III. NUMERICAL RESULTS FOR MODULATED VORTEX PAIRS

Numerical solutions of Eqs. (7) show that only a few trajectory forms are possible. The most important ones can be found by keeping the parameters constant and varying only one initial condition. A common feature of almost all trajectories is that they repeat their shape in λ and also in time. The corresponding temporal period of a trajectory will be denoted by T_0 .

First we investigate type I pairs characterized by some fixed value of φ_r . We vary the initial latitudinal angle φ_0 and choose $\alpha_0 = 0$ which implies an eastward initial velocity. The numerically obtained trajectory forms are shown in Fig. 1. At $\varphi_0 = \varphi_r$ [Fig. 1(a)], a small amplitude meandering motion, called wobbling, is initiated. Increasing φ_0 makes the amplitude also increase [Fig. 1(b)], and a manifestly wobbling motion occurs. The deviation from the eastward direction can grow so large that the trajectory turns back, to the west, intersecting itself [Fig. 1(c)]. This new type of motion is called tumbling. Increasing φ_0 further, we find a critical value φ_c corresponding to a separatrix [Fig. 1(d)] when the trajectory asymptotically approaches a special latitude, denoted by $\varphi_- (\approx \varphi_r)$, corresponding to uniform westward propagation. For $\varphi_0 < \varphi_c$, the motion extends to both sides of φ_- , while for $\varphi_0 > \varphi_c$, the vortices stay on the northern side of φ_- , tracing out tumbling loops [Fig. 1(e), dashed (red) curve]. All the forms described here are repeated in reverse order, in a mirrored way, when initiated well below φ_r [Fig. 1(e), dot-dashed curve, and Fig. 1(f), which represents in a topological sense a mirrored pair to Fig. 1(c)]. There exists another special latitude $\varphi_+ (< \varphi_r$ on the Northern Hemisphere)

which as an initial condition belongs to a uniform eastward propagation. Vortex pairs initiated near φ_+ with an eastward velocity always exhibit a wobbling motion. Whether the trajectory initially bends to the south or to the north depends on whether φ_0 is on the northern or the southern side of φ_+ .

One might note an interesting analogy between the dynamics of a type I pair with any fixed value of φ_r and that of a single inertial orbit on a rotating Earth worked out by Paldor and co-workers [18–22]. The center-of-mass orbits of Fig. 1 are remarkably similar to the ones shown in Fig. 1 of Ref. [18]. This is surprising since the equations of motion are rather different.

The trajectory of a point mass is determined by its initial coordinates and velocity. In order to explore the analogy described above, we have to express the velocity \mathbf{u} of the center of mass of the vortex pair in terms of the positions and the circulations of the elements of the pair. Assuming that the signs of the circulations of the elements are opposite, the dimensionless velocity modulus of the center of mass at any instant of time is given by the average of the velocity moduli of the elements of the pair, after taking into account the spherical geometry:

$$\begin{aligned} |\mathbf{u}(t)| &= \frac{|\Gamma'_1(\varphi_1(t))| + |\Gamma'_2(\varphi_2(t))|}{4\pi D' \sqrt{1 - (D'/2)^2}} \\ &= \frac{2\Gamma' + a'^2\pi (\sin \varphi_2(t) - \sin \varphi_1(t))}{4\pi D' \sqrt{1 - (D'/2)^2}}. \end{aligned} \quad (12)$$

The direction of the velocity is perpendicular to the line connecting the vortices.¹

Now we turn to the investigation of type II pairs. Numerical studies indicate that varying the initial latitude φ_0 for $\alpha_0 = 0$ (similarly as we did for type I pairs, which now implies the variation of the reference latitudes) leads to the appearance of only one trajectory shape, an eastward wobbling. The amplitude of this wobbling increases with increasing φ_0 .

¹To facilitate comparison with Ref. [18], we choose $|\mathbf{u}| \ll 1$, a range motivated in Ref. [18] by geophysical considerations.

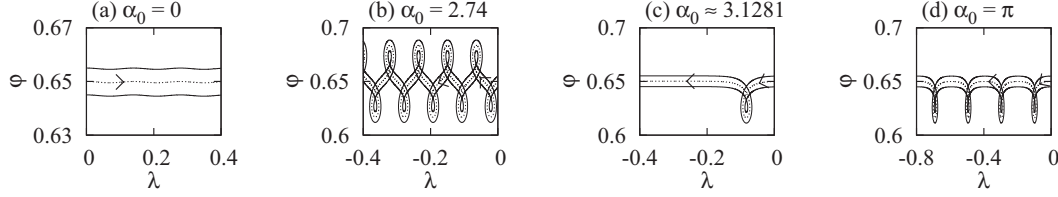


FIG. 2. Trajectories of the vortices (solid lines) and of their centers of mass (dotted line) on the (λ, φ) plane for type II pairs, when varying the initial angle α_0 . The arrows indicate the direction of propagation. (c) A separatrix. Parameters: $D' = 0.01$, $a' = 0.01$, $\Gamma' = 5 \times 10^{-6}\pi$. Initial conditions: $\lambda_0 = 0$, $\varphi_0 = 0.65$, and α_0 as indicated in the panels.

The similarity to the geodesic motion is more hidden: the other trajectory forms can be obtained by varying α_0 at some prescribed value of φ_0 . The numerical results in Fig. 2 indicate that every shape of Fig. 1 appears this way. Note that the tumbling circles exhibit here a left-curving shape, which is characteristic for the type I pairs (shown in Fig. 1) in domains lying on the southern side of the special latitude φ_- . Meanwhile, the wobbling trajectory in Fig. 2(a) bends initially to the right, which is characteristic of the northern side of φ_+ in Fig. 1.

IV. EQUATIONS OF MOTION FOR A DIPOLE

In order to unfold the essence of the vortex dynamics, in this section we consider dipoles, very close and very weak vortex pairs whose velocity is finite. In view of Eq. (12), we are interested in the limit $\Gamma', D' \rightarrow 0$. As a' refers to the radius of a patch of vorticity, for nearby vortices it should also go to zero. Since both D' and a' correspond to distances, we consider them to be of the same order. Let us write the time-dependent vortex coordinates as $\varphi_{1,2} = \varphi \pm d\varphi$, and $\lambda_{1,2} = \lambda \pm d\lambda$, where φ and λ are the center-of-mass coordinates in the dipole limit. For a dipole, $d\varphi$ and $d\lambda$ are infinitesimally small, and we assume that $d\varphi, d\lambda, D', a'$, and Γ' are all of the same order. For a type I pair, no further quantities should be considered as infinitesimally small in the dipole limit. For a type II pair, however, the initial value $d\varphi_0$ of the variable $d\varphi$ takes a special role since the reference latitudes should be written as $\varphi_{1,2r} = \varphi_0 \pm d\varphi_0$ with $d\varphi_0$ infinitesimally small.

From the equations of motion (7) of a vortex pair one can obtain the equations of motion for φ , $d\varphi$, λ , and $d\lambda$ via a systematic Taylor expansion up to leading order. An important element is that the circulations of the vortices have to be calculated up to second order. For a type I pair, the circulations are

$$\begin{aligned} \Gamma'_{1,2}(\varphi_{1,2}) &= \pm\Gamma' + a'^2\pi \sin \varphi_r - a'^2\pi \sin(\varphi \pm d\varphi) \\ &\simeq \pm\Gamma' + a'^2\pi \sin \varphi_r - a'^2\pi \sin \varphi. \end{aligned} \quad (13)$$

For a type II pair, they are written as

$$\begin{aligned} \Gamma'_{1,2}(\varphi_{1,2}) &= \pm\Gamma' + a'^2\pi \sin(\varphi_0 \pm d\varphi_0) - a'^2\pi \sin(\varphi \pm d\varphi) \\ &\simeq \pm\Gamma' + a'^2\pi \sin \varphi_0 - a'^2\pi \sin \varphi. \end{aligned} \quad (14)$$

One finds thus full equivalence between the circulations of type I and type II pairs in the dipole limit with $\varphi_r = \varphi_0$. Since the reference latitudes only appear in the circulations of the

elements, we conclude that the problem of a type II vortex pair in the dipole limit is equivalent to that of a type I dipole with an initial condition $\varphi_0 = \varphi_r$. Alternatively, we can say that the reference latitude of a type I dipole should be chosen as the initial latitude to obtain a type II dipole. Thus, type II dipoles can be regarded as special cases of type I dipoles. In what follows, we only consider type I dipoles and call them dipoles.

From the equations of motion for φ , $d\varphi$, λ , and $d\lambda$, a closed dynamics follows for the center-of-mass coordinates φ and λ :

$$\frac{d}{dt}(\cos \varphi \dot{\lambda}) = \dot{\varphi} \sin \varphi (\gamma \delta(\varphi) + \dot{\lambda}), \quad (15a)$$

$$\frac{d}{dt}\dot{\varphi} = -\dot{\lambda} \cos \varphi \sin \varphi (\gamma \delta(\varphi) + \dot{\lambda}), \quad (15b)$$

where

$$\gamma = \frac{a'^2}{D'^2} \quad (16)$$

and

$$\delta(\varphi) = 1 - \frac{\sin \varphi_r}{\sin \varphi}. \quad (17)$$

The details of the calculation are found in Appendix B. Using the zonal and meridional center-of-mass velocity components

$$u \equiv \dot{\lambda} \cos \varphi, \quad v \equiv \dot{\varphi}, \quad (18)$$

the dynamics of the center of mass is written as

$$\dot{u} = \gamma \delta(\varphi) v \sin \varphi + \tan \varphi u v, \quad (19)$$

$$\dot{v} = -\gamma \delta(\varphi) u \sin \varphi - \tan \varphi u^2.$$

Equations (18) and (19) for a dipole depend only on the parameters φ_r [through the function $\delta(\varphi)$] and $\gamma = a'^2/D'^2$. Γ' does not appear in these equations. Γ' and D' together can be used to set the initial velocity by means of Eq. (12). In the dipole limit, the precise formula is (see Appendix B)

$$|\mathbf{u}| = \frac{\Gamma'}{2\pi D'}. \quad (20)$$

This shows that the velocity modulus can be calculated from the reference vortex strengths.

V. COMPARISON OF DIPOLE AND SINGLE-PARTICLE TRAJECTORIES

In Sec. III, we found a similarity in the shape of the trajectories of a vortex pair to that of a freely moving point

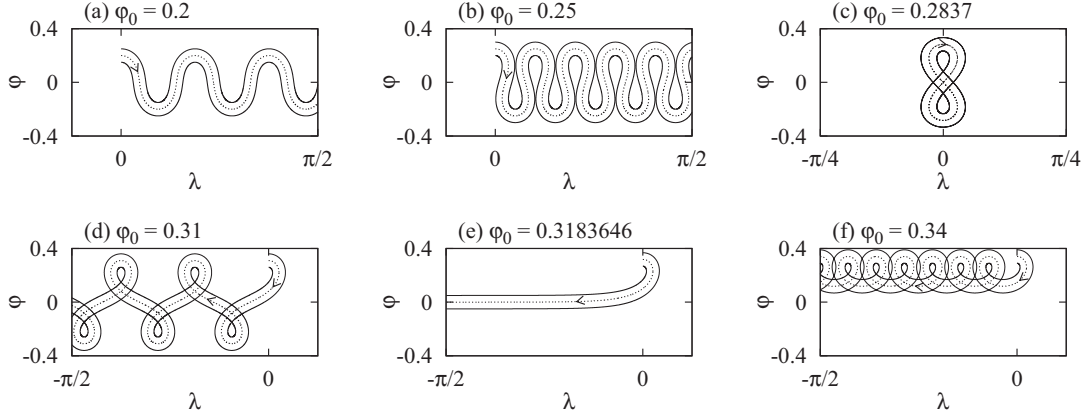


FIG. 3. Trajectories of the vortices (solid lines) and of their center of mass (dotted line) on the (λ, φ) plane for type I pairs with a large distance D' . The arrows indicate the direction of propagation. (c) A figure-eight-shaped trajectory separating net eastward and westward motion. (e) A separatrix. Parameters: $\varphi_r = 0$, $D' = 0.1$, $a' = 0.1$, and $\Gamma' = 0.005\pi$. Initial conditions: $\alpha_0 = 0$, $\lambda_0 = 0$, and φ_0 as indicated in the panels.

mass. Now we show that a full equivalence can be obtained for dipoles at particular values of the parameters φ_r and γ .

The equations of motion for a single particle on a rotating sphere [18] in a form adimensionalized according to the units used so far are

$$\dot{u} = v \sin \varphi + \tan \varphi uv, \quad \dot{v} = -u \sin \varphi - \tan \varphi u^2, \quad (21)$$

$$\dot{\lambda} = \frac{u}{\cos \varphi}, \quad \dot{\varphi} = v, \quad (22)$$

where φ and λ are the geographical coordinates of the point mass, and u and v represent its zonal and meridional velocity components, respectively.

For the equivalence of Eqs. (21) and (22) and Eqs. (18) and (19), we first have to ensure that $\delta(\varphi)$ is 1 independent of φ . This can only be the case if $\varphi_r = 0$, that is, when the reference latitude is at the equator.

With this choice, the equations of motion of the dipole and the single particle are identical, up to the factors of γ . The equivalence is *perfect* if the vortex radius and the vortex distance coincide:

$$a' = D' \quad (23)$$

in the limit of $D' \rightarrow 0$. This may be regarded as a generalization of Kimura's statement [24] on the equivalence of geodesics and vortex dipole trajectories.

When Eq. (23) does not hold, a dipole trajectory does not correspond to a free particle trajectory on the same sphere. However, factor γ can be eliminated by an appropriate rescaling of the dimensionless time, and we can thus say that dipole motion always corresponds to free particle motion on a sphere rotating a factor γ faster than that of the dipole. This also implies that the shape of a dipole trajectory is the same as for a geodesic on a rotating sphere if the reference latitude is $\varphi_r = 0$.

Numerical investigations of the convergence to the dipole limit in the $\varphi_r = 0$, $a' = D'$ case indicate that the difference of the center-of-mass trajectory of a finite size type I vortex pair from the trajectory of a dipole (a geodesic) is negligible when the vortex distance D' is less than 0.001.

The topology of the geodesic trajectories is found to be very robust. Figure 3 shows that we find topologically similar center-of-mass trajectories to those in Fig. 1 of Ref. [18] obtained for free particles even for vortex distance $D' = 0.1$ which is nearly comparable to the radius of the sphere. The trajectories of Fig. 3 are also topologically similar to those obtained with an arbitrary value of φ_r (see Fig. 1). The special feature of the $\varphi_r = 0$ case is that every trajectory has an exactly symmetrical counterpart with respect to the equator, and that the equator coincides with the special latitudes φ_{\pm} that correspond to the uniform eastward and westward propagation, respectively. Both properties follow from Eqs. (18) and (19).

VI. ADVECTION IN THE FIELD OF MODULATED VORTEX PAIRS

A. Introduction

In a frame co-moving with a modulated vortex pair, the flow field is time periodic (with period T_0) and, therefore, the advection dynamics is typically chaotic [25–33]. [An exception is the case of the separatrix motion of Fig. 3(e).] A feature of interest that remains is the type of advective chaos.

There exist two basically different types of advective chaos: that taking place in closed containers [25–28] and that generated by open flows [29,31–33]. In open flows there is a current flowing through the observation region to which particles, once escaped downstream, cannot return. The basic difference between the transport generated by closed and open flows is that particles remain trapped forever around the vortices in the first case, whereas they become transported in the far wake in the second case.

The dynamics of a passive tracer can be considered as that of a third vortex of zero circulation, $\Gamma'_3(\varphi_3) \equiv 0$. We deal then with a restricted three-vortex problem where the inactive vortex has no influence on the others. For illustrative purposes we consider type I vortex pairs with the reference latitude at the equator, $\varphi_r = 0$, and with a relatively large distance D' . The dimensionless equations of motion for the coordinates (φ, λ)

of the tracer particle are thus

$$\frac{d\varphi}{dt} = \frac{1}{4\pi} \sum_{j=1}^2 \frac{(\Gamma' - a^2\pi \sin \varphi_j) \cos \varphi_j \sin(\lambda - \lambda_j)}{1 - \cos \gamma_j}, \quad (24a)$$

$$\frac{d\lambda}{dt} = \frac{1}{\cos \varphi} \frac{1}{4\pi} \sum_{j=1}^2 \frac{(\Gamma' - a^2\pi \sin \varphi_j) [\cos \varphi \sin \varphi_j - \sin \varphi \cos \varphi_j \cos(\lambda - \lambda_j)]}{1 - \cos \gamma_j}, \quad (24b)$$

where

$$\cos \gamma_j = \sin \varphi \sin \varphi_j + \cos \varphi \cos \varphi_j \cos(\lambda - \lambda_j) \quad (25)$$

is related to the chord distance between the tracer and vortex j . Note that the dynamics (24) of a tracer can be considered a dynamical system of two variables driven by the vortex pair dynamics.

On the one hand, we may naively follow the positions of the tracers on the sphere in the original reference frame. On the other hand, the closed-open character of the flow can best be recognized in a reference frame co-moving with the vortex centers. The origin in the λ coordinate is chosen to be the center of mass of the vortex pair (i.e., vortices 1 and 2). In this co-moving reference frame the forcing entering into the two-variable tracer dynamics turns out to be periodic. This allows us to define a two-variable stroboscopic map fully describing the tracer dynamics, taken at integer multiples of T_0 . Consequently, this can be chosen to correspond to a configuration in which the maximum of the vortex center-of-mass trajectory is reached.

From the point of view of the tracer advection, there is always a region close to any of the vortices which is isolated from the surroundings. Here the circulatory flow of a single vortex dominates, and the influence of the other can practically be neglected [34–36]. These regions are called the vortex cores. Whether advection is chaotic is determined by investigating regions outside the cores, but being not far away from the vortices. In between the vortices one always finds such a region because the vortex cores obviously cannot overlap.

If the tracers of a small droplet placed in between the vortices at $t = 0$ remain distributed in a finite range around the vortices after arbitrarily long times, the flow is closed; otherwise it is open. From a dynamical-systems point of view, the basic difference between closed and open advection dynamics lies in the structure of the chaotic set. For closed chaotic advection, which is an example of a closed Hamiltonian chaos, the chaotic set extends over a two-dimensional area of the fluid surface. The region filled in asymptotically by the droplet points is part of the chaotic set, and other such areas might also exist, reachable from other initial droplet positions. In contrast, the chaotic invariant set of the open advection dynamics contains fractal parts of zero area. This chaotic saddle [31,32,37,38] is formed by an infinity of unstable particle orbits which are trapped by the vortices forever, both forward and backward in time. In such cases points of a droplet come to a close neighborhood of the chaotic saddle, but leave it sooner or later. Their asymptotic form is determined by the unstable manifold [31–33,37,38], itself a fractal, of the chaotic saddle.

B. Short term advection

In order to study the short term advection dynamics, we initiate a small droplet of tracer particles between the two vortices and follow its evolution. One option is to plot the positions of the tracers after some time to visualize the spatial pattern characterizing the advection process (i.e., the unstable manifold of the saddle in the open case). As another option, we define an escape circle of radius ρ centered in the center of mass of the two vortices and measure the escape time (the time needed to leave the circle) of each tracer. We choose this radius ρ to be considerably smaller than the diameter of the sphere in order to ensure that the tracers detrained along the wake leave the escape circle before they could reenter again. This way we investigate the short term detrainment of the tracers from the neighborhood of the pair. High escape times from the circle correspond to closed advection and to initial conditions situated either in the vortex cores or close to the stable manifold of the chaotic saddle in the case of open advection. Plotting the escape time as a function of the initial position thus draws out the stable manifold of the saddle as ridges in the plot.

When numerically investigating the advection generated by vortex pairs initiated with an eastward velocity, we find that the open or closed character of the flow can be altered by a mere change in the initial latitude (as also found on a topographic β plane in Ref. [12]). Vortex initial conditions closer to the equator than this critical latitude φ_{0c} lead to open advection, while the others correspond to closed advection.

Numerical results are presented in Figs. 4 and 5. For wobbling motion [Fig. 4] the tracers are detrained along a simple tail; an intricate lobe structure is not recognizable (without magnification). When the vortex trajectories cross themselves [Fig. 4(b)], large lobes are formed on both sides of the equator in a symmetrical manner. Finally, when the trajectory is tumbling and is confined to one of the hemispheres [Fig. 4(c)], southward traveling lobes are created. In each case the fractal pattern of the stable manifold of the saddle can be seen as filamentary structures in the escape time distributions [Figs. 5(a)–5(c)]. Above a critical initial latitude $\varphi_{0c} \approx 0.40$, the tracers are confined to the neighborhood of the vortices [Fig. 4(d)], and the advection dynamics becomes closed. It is worth noting that the critical latitude φ_{0c} differs from the separatrix latitude φ_c defined for the vortex pair dynamics.

C. Time scale separation and crossover to global mixing

It is an interesting consequence of spherical topology that the open character seen on short time scales crosses over into a closed advection for asymptotically long times. The reason for this is that the vortex pair meets its wake after one global

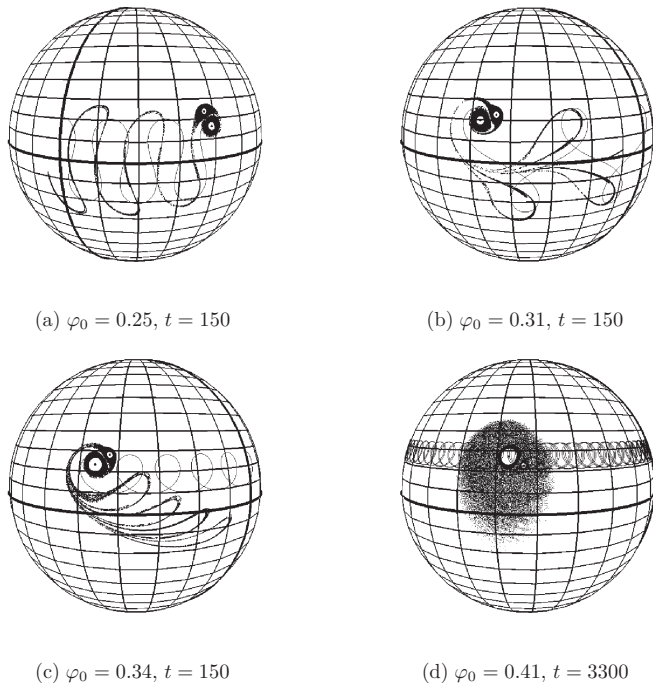


FIG. 4. Positions of $N \approx 70\,000$ advected tracers and the two vortices (denoted by larger dots) at time t . The center-of-mass trajectory of the vortices [corresponding to motions shown in planar representation in Figs. 3(b), 3(d), 3(f), and 5(d)] is marked by a thin solid line. Thick lines indicate the equator and the $\lambda = 0$ meridian. The tracers were initiated at the colored and the light gray grid points in Fig. 5. Vortex pair parameters: $\varphi_r = 0$, $D' = 0.1$, $a' = 0.1$, and $\Gamma' = 5 \times 10^{-3}\pi$. Vortex initial conditions: $\alpha_0 = 0$, $\lambda_0 = 0$, and φ_0 as indicated in the panels.

period T_1 corresponding to the time needed for the vortex pair to go around the sphere. The characteristic periods T_0 and T_1 are rather different [in the case of Fig. 4(a) they are

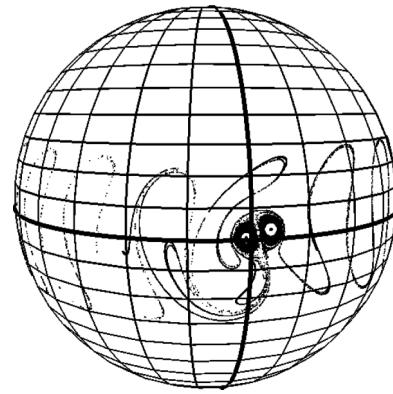


FIG. 6. Positions of $N \approx 70\,000$ advected tracers at $t = 1000 \approx T_1$. The fact that the center of mass of the vortices has just passed the $\lambda = 0$ meridional indicates that the time taken is slightly more than one global period T_1 . The tracers were initiated at the colored and the light gray grid points in Fig. 5(a). Vortex pair parameters: $\varphi_r = 0$, $D' = 0.1$, $a' = 0.1$, and $\Gamma' = 5 \times 10^{-3}\pi$. Vortex initial conditions: $\alpha_0 = 0$, $\lambda_0 = 0$, and $\varphi_0 = 0.25$.

$T_0 = 50.6$ and $T_1 \approx 988$, respectively]; therefore, qualitatively different advection patterns are expected on the time scales $t \leq T_1$ and $t \gg T_1$. As the vortex pair propagates through its own wake, it mixes the tracers which already went through a similar process when they were located in the vicinity of the vortex pair one global period earlier. This is numerically illustrated in Figs. 6 and 7, in a spherical view and in a planar representation, respectively. After several such mixing events we find the tracers to continuously fill a zonal band around the sphere [see Fig. 7(b)]. This band is somewhat narrower near the current location of the vortex pair. By time $t = 11\,050$ the band is populated by a nearly space-filling distribution, indicating the tendency towards a complete mixing. The slight increase of the density of tracers in some localized region in

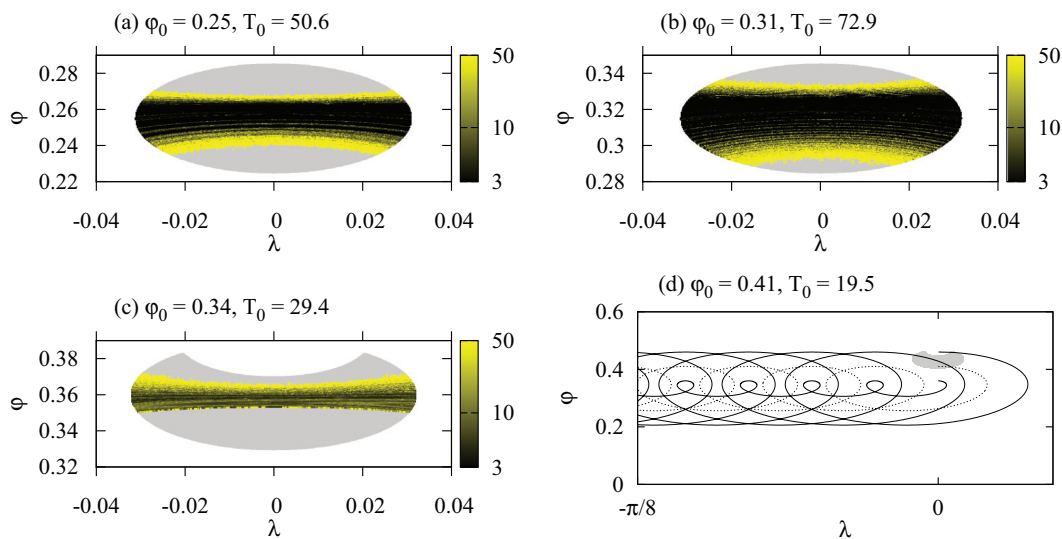


FIG. 5. (Color online) Escape times (indicated on the color scale, measured in units of the time period T_0 for an escape radius $\rho = 0.8$) of the tracers of Fig. 4, as a function of their initial position. Homogeneous light gray color indicates that the corresponding tracers did not leave the neighborhood of the vortices during the simulation time of $250T_0$. φ_0 and T_0 are indicated in the panels. (d) The closed case. It presents the shape of the initial tracer droplet in homogeneous light gray color. The trajectories of the vortices (solid lines) and of their centers of mass (dotted line) are also shown to help visualize the relative size and location of the droplet compared to the vortex motion.

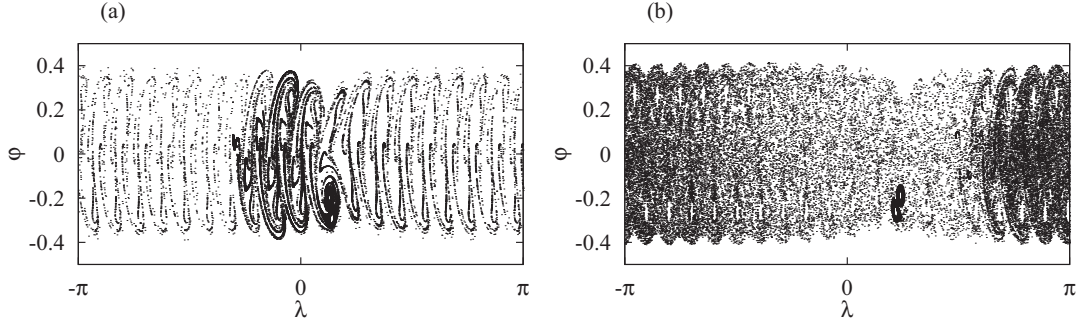


FIG. 7. Same as Fig. 6 for (a) $t = 2050 \approx 2T_1$ and (b) $t = 11050 \approx 11T_1$ in a planar view.

λ is a consequence of the initially localized tracer distribution and will slowly disappear with a further increase of time.

The easiest way to characterize these phenomena is the investigation of a chaotic scattering process [31,37,38] in the stroboscopic map defined in Sec. VIA in a reference frame co-moving with the vortices. On the map's surface in this reference frame the fluid moves uniformly (in zonal direction) except for the vicinity of the $\lambda = 0$ coordinate where the vortex pair is located in a meridional direction. Chaotic features in the tracer advection can only occur in this localized region. One can thus define this region as a scattering region. Due to the zonal direction of the uniform movement of the fluid far from the origin, one may decide to rely only on the coordinate λ when declaring boundaries for the scattering region: we define this region as the interval $\lambda \in (-\lambda_b, \lambda_b)$, indicated in Fig. 8.

The investigation of the short term behavior corresponds to taking into account only one scattering event for some particular tracer. We call this scattering process an elementary scattering. This elementary scattering event is characterized by a chaotic saddle localized near the vortices, which we call the elementary saddle. It has stable and unstable manifolds which extend outside the scattering region.

The elementary saddle and its invariant manifolds can be numerically constructed by the application of the sprinkler method [38]: we initiate a droplet of tracers in the incoming asymptotic region and start a time counter when they first step inside the scattering region. We stop the counter when they leave the scattering region to obtain a (discrete) delay time for each tracer. Particles with a large delay time approach the ele-

mentary saddle during the scattering event. Therefore, their positions in the incoming asymptotic region mark the stable manifold of this saddle.² Their positions corresponding to about half time of the scattering process trace out the elementary saddle, and their positions in the outgoing asymptotic region represent the unstable manifold of this saddle.³ As a first approach, we only follow the evolution of the tracers up to their first encounter with $\lambda = -\pi$. We show the corresponding results in Fig. 8(a). The tracers are detrained from the vicinity of the vortex pair along the unstable manifold [marked by light gray (red) in Fig. 8(a)] of the elementary saddle. The elementary saddle itself can be considered the intersection of its own stable and unstable manifolds [although this is not visible in Fig. 8(a) since we do not plot the manifolds for $|\lambda| < \lambda_b$ for clarity].

Due to the periodic nature of the sphere in λ , the invariant manifolds do not have an end at π or $-\pi$ but they reenter the domain $\lambda \in [-\pi, \pi)$ on the other side. If we just follow them up to their next encounter with the interval $(-\lambda_b, \lambda_b)$ (without taking into account a second scattering event), we find that they *intersect* each other. The creation of new homoclinic and

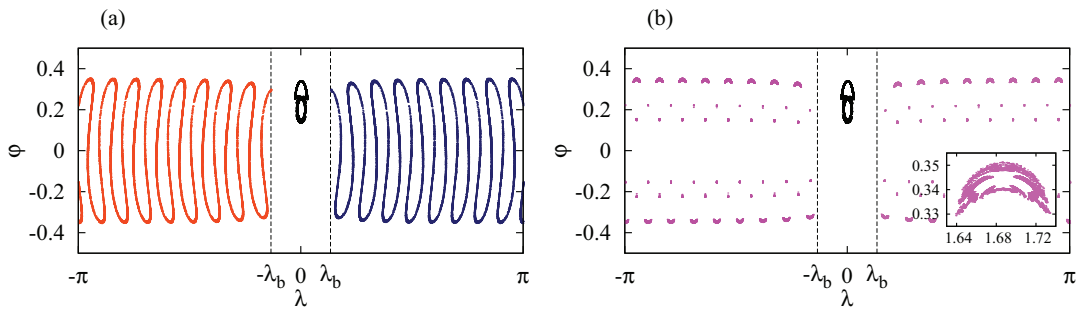


FIG. 8. (Color online) (a) The stable (blue or dark gray) and unstable (red or light gray) manifold of the elementary saddle, followed up to $\lambda = \pi$ and $-\pi$, respectively. The elementary saddle is shown in black in the scattering region $\lambda \in (-\lambda_b, \lambda_b)$. These sets are numerically obtained by means of the sprinkler method with $N = 1.9 \times 10^6$ tracers. (b) The new components (magenta or gray) of the chaotic saddle as described in the text, obtained as intersection points between the stable and the unstable manifolds of the elementary saddle. For comparison the elementary saddle is also plotted. The inset in (b) is a magnification of a well-populated region of the new saddle components. Vortex pair parameters: $\varphi_t = 0$, $D' = 0.1$, $a' = 0.1$, and $\Gamma' = 5 \times 10^{-3} \pi$. Vortex initial conditions: $\alpha_0 = 0$, $\lambda_0 = 0$, and $\varphi_0 = 0.25$. $\lambda_b = 0.42$.

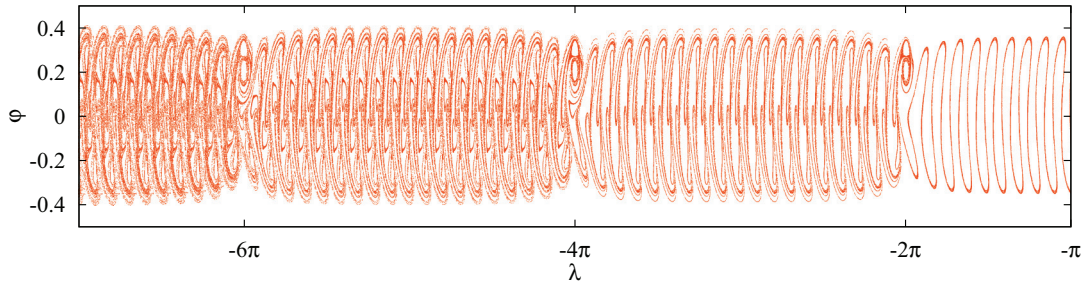


FIG. 9. (Color online) The unstable manifold of the elementary saddle, plotted in subsequent windings around the sphere by defining λ as a rotational angle.

heteroclinic points implies the appearance of new components of the chaotic saddle underlying the dynamics on long time scales. These new components consist of orbits which are permitted to leave the close vicinity of the vortices but return after the number of iterations that corresponds to one winding around the sphere. Note that the investigated intersections of the stable and the unstable manifold of the elementary saddle appear *in the whole domain* $\lambda \in [-\pi, \pi]$ [i.e., also outside $(-\lambda_b, \lambda_b)$], implying that the chaotic saddle has a zonally *global* extension. This is illustrated in Fig. 8(b). In the inset of Fig. 8(b) one can see the fractal structure of the new components of the chaotic saddle.

The stable and unstable manifolds of the elementary saddle do not have an end even after one full winding (once around the entire sphere). After each full winding new intersection points are created. For simplicity, let us suppose that the invariant manifolds of the elementary saddle do not change their spatial pattern shown in Fig. 8(a) when continuing the manifolds arbitrarily long. Since the ratio T_0/T_1 of the local and global periods is typically irrational, the created intersection points will densely fill the whole domain $\lambda \in [-\pi, \pi]$ in the limit of infinitely many windings.

The real scenario is, however, more complicated. For convenience, let us define λ as a rotational angle to see clearly how the invariant manifolds of the elementary saddle evolve after subsequent windings. In Fig. 9, one can observe that the unstable manifold of the elementary saddle is distorted (or mixed) when meeting the vortices at $\lambda = -2\pi$. Every time the invariant manifolds of the elementary saddle meet the vortices it results in a mixing due to chaotic effects originating from the elementary scattering. After such an event the invariant manifolds cannot become less dense than before mixing. This process repeats itself at integer multiples of -2π . As a consequence, the argument corresponding to the simplified scenario remains valid and the full domain $\lambda \in [-\pi, \pi]$ becomes densely filled by intersection points in the limit of infinitely many windings in the real scenario as well. This implies that the exact chaotic “saddle” of the full global problem of tracer advection is space filling. This corresponds to a chaotic sea characterizing the asymptotically long time advection of the tracers in the velocity field of a vortex pair. The space-filling behavior starts to emerge on time scales much longer than the global period T_1 .

Since a drop of tracers of any shape is smeared into a space-filling distribution after a long time, this is true also for the simple pattern of the unstable manifold of the elementary scattering shown in Fig. 8(a). We can see three steps of this

process in Fig. 9: the unstable manifold becomes denser when crossing integer multiples of 2π from the right to the left. This shows that the transition to a space-filling distribution is a step-by-step process, controlled by the elementary scattering. From Fig. 9 one also learns that the chaotic sea only extends to a finite interval in the latitudinal variable φ : though the unstable manifold expands in φ at $\lambda = -2\pi$, the expansions occurring later are weaker, and the width converges to a finite size. Then we can say that the long term global advection is characterized by a chaotic sea that extends to a whole zonal band on the sphere.

It is important to note that this conclusion is true only in cases when the short term tracer advection is open. If the short term advection is closed, the invariant manifolds of the chaotic set do not leave the vicinity of the vortices and the chaotic set remains localized around the vortices in both λ and φ . This implies that tracers initiated near the vortices always stay in a localized region around the vortices and never fill a whole zonal band [see Fig. 4(d)].

VII. SUMMARY

In order to find a phenomenological model of vortices on a rotating sphere, we have extended the concept of modulation to spherical geometry by taking into account the preservation of potential vorticity. The new modulation implies a sinusoidal dependence of the vortex circulation on the latitudinal angle.

We have unfolded the nontrivial dynamics of modulated vortex pairs and have found a qualitative similarity to the free particle motion on a rotating sphere. In the dipole limit, when both the vortex strength Γ and the distance D between the vortices is very small, but their ratio, a characteristic velocity, is finite, a full equivalence is found for the special choice when the vortex radius a coincides with D and the reference latitude is the equator $\varphi_r = 0$. In other cases, the vortex trajectories are deformed versions of those of free particles.

Advection in the velocity field of modulated vortex pairs is studied by considering the passive tracers as vortices of identically zero circulation. The advection dynamics is typically chaotic, which would not be the case on a nonrotating sphere. We find a transition from closed to open chaotic advection in the field of vortex pairs when the initial latitude of the pair becomes closer to the reference latitude than a threshold distance. On asymptotically long times, however, even the open advection becomes converted into a closed one since the vortex pair periodically reenters its own wake due to spherical topology. The chaotic saddle governing the open dynamics gradually becomes space filling. Such a time scale separation is

expected to occur in any chaotic advection problem where the flow is locally open but globally closed. Relevant situations are provided by the advection by planar vortex pairs moving inside a disk [39], and when understanding mixing in an infinite array of cylinders, as defined in Ref. [40], based on the elementary saddle formed in the wake of a single cylinder [31].

In another vein, our approach indicates that previous studies of point vortices on a sphere, which were mainly devoted to the stability of different vortex configurations (see, e.g., [3–6,41–45]), might be worth extending to dynamical cases. Both these and the vortex pair dynamics understood on general curved surfaces [24,46] would be highly interesting to investigate in the presence of rotation.

ACKNOWLEDGMENTS

Helpful discussions with Stefanello Boatto, Nathan Paldor and Tímea Haszpra are acknowledged. The project is supported by the European Union and co-financed by the European Social Fund (Grant No. TAMOP 4.2.1./B-09/1KMR-2010-0003), as well as by OTKA (Grant No. NK100296). T. Tél acknowledges the support of the Alexander von Humboldt Foundation.

APPENDIX A: DISTANCE BETWEEN A VORTEX COUPLE

The equations of motion (4) for the locations \mathbf{r}_1 , \mathbf{r}_2 of two vortices of arbitrary modulation can also be written in vectorial form [1]:

$$\begin{aligned}\dot{\mathbf{r}}_1 &= \frac{1}{2\pi} \Gamma_2(\varphi_2) \frac{\hat{\mathbf{n}}_2 \times (\mathbf{r}_1 - \mathbf{r}_2)}{r_{12}^2}, \\ \dot{\mathbf{r}}_2 &= \frac{1}{2\pi} \Gamma_1(\varphi_1) \frac{\hat{\mathbf{n}}_1 \times (\mathbf{r}_2 - \mathbf{r}_1)}{r_{12}^2},\end{aligned}\quad (\text{A1})$$

$$\frac{d}{dt}(\varphi \pm d\varphi) = \frac{[\Gamma'(\varphi \mp d\varphi)] \cos(\varphi \mp d\varphi) \sin(\pm 2d\lambda)}{2\pi D^2}, \quad (\text{B1a})$$

$$\frac{d}{dt}(\lambda \pm d\lambda) = \frac{\Gamma'(\varphi \mp d\varphi) \cos(\varphi \pm d\varphi) \sin(\varphi \mp d\varphi) - \sin(\varphi \pm d\varphi) \cos(\varphi \mp d\varphi) \cos(\pm 2d\lambda)}{2\pi D^2 \cos(\varphi \pm d\varphi)}. \quad (\text{B1b})$$

Note that these are in fact four equations. As a first step, we determine the right-hand side of this system of equations up to first order. Since D^2 , appearing in the denominator, is a quantity of second order, one can see, after expanding the trigonometric expressions up to first order, that the circulations (in the numerators on the right-hand side) should be calculated up to second order. Therefore, the result (13) for the circulation of an element of a dipole can be substituted. As a next step, we express $\dot{\varphi}$, $\dot{d}\varphi$, $\dot{\lambda}$, and $\dot{d}\lambda$:

$$\dot{\varphi} = -\frac{1}{\pi D^2} \Gamma' \cos \varphi d\lambda, \quad (\text{B2a})$$

$$\dot{d}\varphi = -\frac{1}{\pi D^2} [\Gamma' d\varphi + a^2 \pi \delta(\varphi) \cos \varphi] \sin \varphi d\lambda, \quad (\text{B2b})$$

$$\dot{\lambda} = \frac{1}{\cos \varphi} \frac{1}{\pi D^2} \Gamma' d\varphi, \quad (\text{B2c})$$

where $\hat{\mathbf{n}}_i$ is the normal vector to the sphere at the location of vortex i . Expressing the square of the chord distance in vectorial form and taking its temporal derivative,

$$\begin{aligned}\frac{d}{dt}(r_{12}^2) &= \frac{d}{dt}[(\mathbf{r}_1 - \mathbf{r}_2)^2] = -2 \frac{d}{dt}(\mathbf{r}_1 \mathbf{r}_2) \\ &= -2(\dot{\mathbf{r}}_1 \mathbf{r}_2 + \mathbf{r}_1 \dot{\mathbf{r}}_2).\end{aligned}\quad (\text{A2})$$

By substituting Eq. (A1) we obtain

$$\begin{aligned}\frac{d}{dt}(r_{12}^2) &= -\frac{1}{\pi r_{12}^2} \Gamma_2(\varphi_2) \left[\hat{\mathbf{n}}_2 \times (\mathbf{r}_1 - \mathbf{r}_2) \right] \mathbf{r}_2 \\ &\quad - \frac{1}{\pi r_{12}^2} \Gamma_1(\varphi_1) \mathbf{r}_1 \left[\hat{\mathbf{n}}_1 \times (\mathbf{r}_2 - \mathbf{r}_1) \right] \\ &= -\frac{1}{\pi r_{12}^2} \Gamma_2(\varphi_2) \left[\mathbf{r}_2 \times \frac{\mathbf{r}_2}{R} \right] (\mathbf{r}_1 - \mathbf{r}_2) \\ &\quad - \frac{1}{\pi r_{12}^2} \Gamma_1(\varphi_1) \left[\mathbf{r}_1 \times \frac{\mathbf{r}_1}{R} \right] (\mathbf{r}_2 - \mathbf{r}_1) = 0\end{aligned}\quad (\text{A3})$$

since the product of parallel vectors is zero. The chord distance D of a two-vortex system is thus always constant on a sphere of arbitrary rotation.

APPENDIX B: DERIVATION OF THE DIPOLE EQUATIONS

The dimensionless equations of motion (7) are written for an infinitesimally small vortex pair as

$$\dot{d}\lambda = \frac{1}{\pi D^2} \left[\Gamma' \left(\frac{d\varphi^2}{\cos^2 \varphi} - d\lambda^2 \right) + a^2 \pi \delta(\varphi) \frac{d\varphi}{\cos \varphi} \right] \sin \varphi, \quad (\text{B2d})$$

where

$$\delta(\varphi) = 1 - \frac{\sin \varphi_r}{\sin \varphi}. \quad (\text{B3})$$

(Note that $\lim_{\varphi \rightarrow 0} \delta(\varphi) = \pm\infty$; the right-hand sides of Eqs. (B2b) and (B2d), however, always remain finite.) One can see that the left- and the right-hand sides of any of Eqs. (B2a)–(B2d) are of the same order.

Taking the first temporal derivative of Eqs. (B2a) and (B2c) leads to

$$\frac{d}{dt} \dot{\varphi} = \frac{1}{\pi D^2} \Gamma' \sin \varphi \dot{\varphi} d\lambda - \frac{1}{\pi D^2} \Gamma' \cos \varphi \dot{d}\lambda, \quad (\text{B4a})$$

$$\frac{d}{dt} (\cos \varphi \dot{\lambda}) = \frac{1}{\pi D^2} \Gamma' \dot{d}\varphi. \quad (\text{B4b})$$

Expressing the derivatives $\dot{\varphi}$, $d\lambda$, and $d\varphi$ on the right-hand side from the system (B), we arrive at Eq. (15).

In view of Eq. (18), the velocity components (u, v) of the center of mass of the dipole are obtained from Eqs. (B2a) and (B2c) as

$$u = \frac{1}{\pi D^2} \Gamma' d\varphi, \quad (\text{B5a})$$

$$v = -\frac{1}{\pi D^2} \Gamma' \cos \varphi d\lambda. \quad (\text{B5b})$$

The velocity modulus is thus

$$|\mathbf{u}| \equiv \sqrt{u^2 + v^2} = \frac{\Gamma'}{\pi D^2} \sqrt{d\varphi^2 + \cos^2 \varphi d\lambda^2} = \frac{\Gamma'}{2\pi D'}, \quad (\text{B6})$$

since

$$D'^2 = 2(1 - \cos \gamma_{12}) = 4(d\varphi^2 + \cos^2 \varphi d\lambda^2). \quad (\text{B7})$$

-
- [1] P. K. Newton, *The N-Vortex Problem: Analytical Techniques* (Springer, Berlin, 2001).
- [2] P. K. Newton and S. D. Ross, *Phys. D (Amsterdam, Neth.)* **223**, 36 (2006).
- [3] M. I. Jamaloodeen and P. K. Newton, *Proc. R. Soc. London, Ser. A* **462**, 3277 (2006).
- [4] P. K. Newton and H. Shokrane, *Proc. R. Soc. London, Ser. A* **462**, 149 (2006).
- [5] P. K. Newton and T. Sakajo, *Proc. R. Soc. London, Ser. A* **463**, 961 (2007).
- [6] P. K. Newton and H. Shokrane, *Proc. R. Soc. London, Ser. A* **464**, 1525 (2008).
- [7] M. T. DiBattista and L. M. Polvani, *J. Fluid Mech.* **358**, 107 (1998); L. M. Polvani and D. G. Dritschel, *ibid.* **255**, 35 (1993).
- [8] M. Makino, T. Kamimura, and T. Taniuti, *J. Phys. Soc. Jpn.* **50**, 980 (1981).
- [9] N. J. Zabusky and J. C. McWilliams, *Phys. Fluids* **25**, 2175 (1982).
- [10] D. D. Hobson, *Phys. Fluids A* **3**, 3027 (1991).
- [11] O. U. Velasco Fuentes and G. J. F. van Heijst, *J. Fluid Mech.* **259**, 79 (1994).
- [12] I. J. Benczik, T. Tél, and Z. Köllö, *J. Fluid Mech.* **582**, 1 (2007).
- [13] J. Pedlosky, *Geophysical Fluid Dynamics* (Springer, Berlin, 1979).
- [14] R. C. Kloosterziel, G. F. Carnevale, and D. Philippe, *Dyn. Atmos. Oceans* **19**, 65 (1993).
- [15] O. U. Velasco Fuentes and G. J. F. van Heijst, *Phys. Fluids* **7**, 2735 (1995).
- [16] O. U. Velasco Fuentes, G. J. F. van Heijst, and B. E. Cremers, *J. Fluid Mech.* **291**, 139 (1995).
- [17] O. U. Velasco Fuentes and F. A. Velázquez Muñoz, *Phys. Fluids* **15**, 1021 (2003).
- [18] N. Paldor and P. D. Killworth, *J. Atmos. Sci.* **45**, 4013 (1988).
- [19] N. Paldor and E. Boss, *J. Atmos. Sci.* **49**, 2306 (1992).
- [20] V. Rom-Kedar, Y. Dvorkin, and N. Paldor, *Phys. D (Amsterdam, Neth.)* **106**, 389 (1997).
- [21] Y. Dvorkin and N. J. Paldor, *J. Atmos. Sci.* **56**, 1229 (1999).
- [22] N. Paldor, in *Lagrangian Analysis and Prediction of Coastal and Ocean Dynamics*, edited by A. Griffa, A. D. Kirwan, A. J. Marino, T. Özgökimen, and T. Rossby (Cambridge University Press, Cambridge, 2007), pp. 119–135.
- [23] N. Paldor and A. Sigalov, *Tellus A* **58**, 280 (2006).
- [24] Y. Kimura, *Proc. R. Soc. London, Ser. A* **455**, 245 (1999).
- [25] H. Aref, *J. Fluid. Mech.* **143**, 1 (1984).
- [26] H. Aref, *Phys. Fluids* **14**, 1315 (2002).
- [27] J. M. Ottino, *The Kinematics of Mixing: Stretching, Chaos and Transport* (Cambridge University Press, Cambridge, 1989).
- [28] A. Provenzale, *Annu. Rev. Fluid Mech.* **31**, 55 (1999).
- [29] Z. Neufeld and T. Tél, *Phys. Rev. E* **57**, 2832 (1998).
- [30] A. Daitche and T. Tél, *Phys. Rev. E* **79**, 016210 (2009).
- [31] C. Jung, T. Tél, and E. Ziemniak, *Chaos* **3**, 555 (1993).
- [32] Á. Péntek, T. Tél, and Z. Toroczkai, *J. Phys. A* **28**, 2191 (1995).
- [33] J. C. Sommerer, H.-C. Ku, and H. E. Gilreath, *Phys. Rev. Lett.* **77**, 5055 (1996).
- [34] L. Kuznetsov and G. M. Zaslavsky, *Phys. Rev. E* **58**, 7330 (1998).
- [35] L. Kuznetsov and G. M. Zaslavsky, *Phys. Rev. E* **61**, 3777 (2000).
- [36] X. Leoncini, L. Kuznetsov, and G. M. Zaslavsky, *Phys. Rev. E* **63**, 036224 (2001).
- [37] E. Ott, *Chaos in Dynamical Systems*, 2nd ed. (Cambridge University Press, Cambridge, 2002).
- [38] Y.-C. Lai and T. Tél, *Transient Chaos, Complex Dynamics on Finite-Time Scales* (Springer, New York, 2011).
- [39] L. Zannetti and P. Franzese, *Phys. D (Amsterdam, Neth.)* **76**, 99 (1994).
- [40] M. A. F. Sanjuan, J. Kennedy, C. Grebogi, and J. A. Yorke, *Chaos* **7**, 125 (1997).
- [41] K. A. O'Neil, *Trans. Am. Math. Soc.* **302**, 383 (1987).
- [42] S. Pekarsky and J. E. Marsden, *J. Math. Phys.* **39**, 5894 (1998).
- [43] C. Lim, J. Montaldi, and M. Roberts, *Physica D* **148**, 97 (2001).
- [44] S. Boatto and J. Laskar, *Chaos* **13**, 824 (2003).
- [45] S. Boatto, *Discrete Contin. Dyn. Syst. B* **10**, 349 (2008).
- [46] S. Boatto and J. Koiller (unpublished).